Nuclear Import of the HIV-1 Core Precedes Reverse Transcription and Uncoating

Anastasia Selyutina[1,3], **Mirjana Persaud**[1,3], **Kyeongeun Lee**[2], **Vineet KewalRamani**[2], **Felipe Diaz-Griffero**[1,4,*]

[1]Department of Microbiology and Immunology, Einstein, Bronx, NY 10461, USA

[2]Center for Cancer Research, National Cancer Institute at Frederick, Frederick, MD 21702-1201, USA

[3]These authors contributed equally

[4]Lead Contact

SUMMARY

HIV-1 reverse transcription (RT) occurs before or during uncoating, but the cellular compartment where RT and uncoating occurs is unknown. Using imaging and biochemical assays to track HIV-1 capsids in the nucleus during infection, we demonstrated that higher-order capsid complexes and/or complete cores containing the viral genome are imported into the nucleus. Inhibition of RT does not prevent capsid nuclear import; thus, RT may occur in nuclear compartments. Cytosolic and nuclear fractions of infected cells reveal that most RT intermediates are enriched in nuclear fractions, suggesting that HIV-1 RT occurs in the nucleus alongside uncoating. In agreement, we find that capsid in the nucleus induces recruitment of cleavage and polyadenylation specific factor 6 (CPSF6) to SC35 nuclear speckles, which are highly active transcription sites, suggesting that CPSF6 through capsid is recruiting viral complexes to SC35 speckles for the occurrence of RT. Thus, nuclear import precedes RT and uncoating, which fundamentally changes our understanding of HIV-1 infection.

In Brief

Selyutina et al. show that HIV-1 cores containing the viral genome are imported into the nucleus for reverse transcription and uncoating. HIV-1 cores in the nucleus are recruited by CPSF6 to SC35 highly active transcription domains for viral reverse transcription, integration, and/or expression.

Graphical Abstract
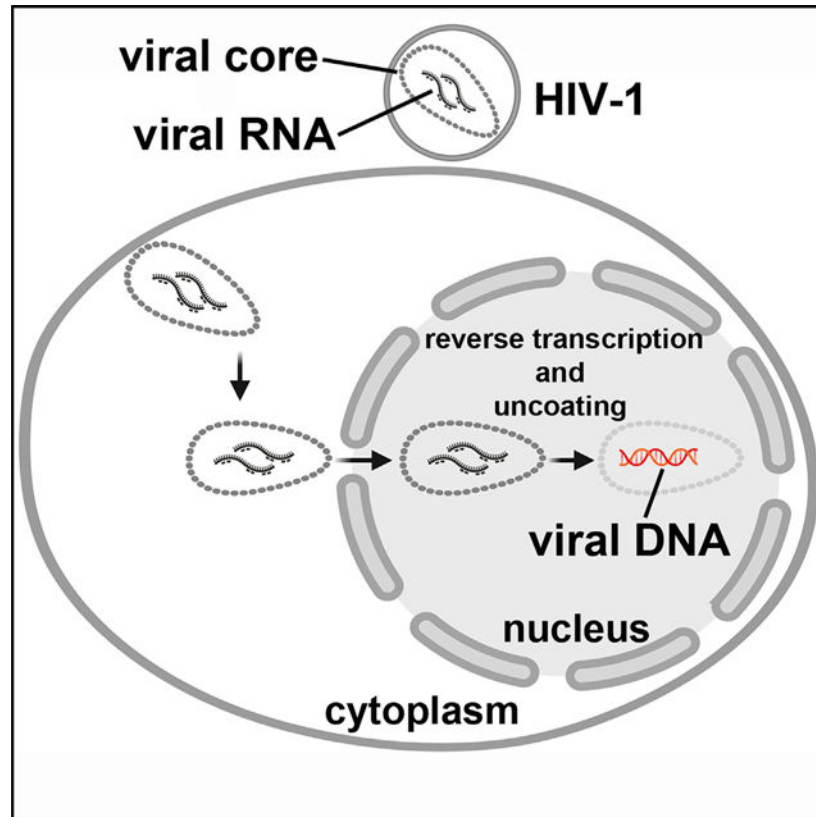
INTRODUCTION

The influence of the physiological state of cells on retroviral replication was initially studied by Rubin and Temin, who demonstrated that stopping cell division by X-rays or UV light prevents Rous sarcoma virus replication (Rubin and Temin, 1959; Temin and Rubin, 1959). Subsequent research established the relationship between cell-cycle stage and retroviral infection, revealing that diverse retroviruses have different requirements for productive infection (Katz et al., 2005; Suzuki and Craigie, 2007; Yamashita and Emerman, 2004, 2005, 2006; Yamashita et al., 2007). Lentiviruses such as HIV-1 show no difference in productive infection when comparing dividing versus nondividing cells (Lewis et al., 1992), suggesting that lentiviruses developed specific mechanisms to reach the nucleus.

Although the ability of HIV-1 to enter the nucleus has been attributed to a variety of viral proteins, it is accepted that capsid plays a dominant role (Yamashita and Emerman, 2004; Yamashita et al., 2007). HIV-1 particles contain a core formed by ~1,500 monomers of capsid protein housing the viral RNA. 40% of the total capsid protein in the viral particle forms the core (Briggs et al., 2003, 2004, 2006). Recent evidence suggested that capsid is required for both reverse transcription (RT) and nuclear import (Hulme et al., 2011; Roa et al., 2012; Yamashita and Emerman, 2004; Yamashita et al., 2007; Yang et al., 2013).

HIV-1 RT occurs inside the viral core before or during uncoating, but not after (Diaz-Griffero et al., 2007; Roa et al., 2012; Stremlau et al., 2006). Inhibition of RT delays HIV-1 uncoating, suggesting that RT initiation is required for uncoating (Hulme et al., 2011; Yang et al., 2013). These experiments implied that complete or partial integrity of the HIV-1 core is required for RT and prompted questioning into the true cellular localization of uncoating and RT.

The use of imaging has revealed the presence of capsid in the nucleus (Bejarano et al., 2019; Chin et al., 2015; Hulme et al., 2015; Peng et al., 2014). Although tracking single particles by fluorescence microscopy has detected HIV-1 replication complexes in the nucleus (Bejarano et al., 2019; Burdick et al., 2017; Francis and Melikyan, 2018), the total amount of capsid in the nucleus and its importance for infection have not been studied. This work therefore sought to explore the importance of nuclear capsid for productive infection.

Using biochemical assays to track the fraction of capsid, we found that assembled capsid complexes are imported into the nuclear compartment. In agreement, inhibition of RT does not prevent capsid import into the nucleus, indicating that RT is occurring in the nuclear compartment. To test this hypothesis, we measured the steps of RT over time. Our results reveal that most of the observable RT intermediates are enriched in the nuclear compartment, inferring that most HIV-1 RT occurs in the nucleus. These experiments also imply that uncoating proceeds in the nuclear compartment. In agreement, we found that the presence of HIV-1 capsid in the nucleus during infection induces recruitment of cleavage and polyadenylation specific factor 6 (CPSF6) to nuclear speckles (SC35), suggesting that CPSF6 through capsid is likely recruiting viral complexes to SC35 speckles for the occurrence of RT. Contrary to the current belief that HIV-1 uncoating and RT occurs in the cytosol, these findings fundamentally change our understanding of HIV-1 infection by showing that nuclear import precedes RT and uncoating.

RESULTS

Biochemical Assay to Detect Capsid in the Nuclei of HIV-1-Infected Human Cells

Tracking single HIV-1 particles by microscopy permitted the detection of capsids in nuclei (Bejarano et al., 2019; Chin et al., 2015; Hulme et al., 2015; Peng et al., 2014); however, the contribution of HIV-1 capsid to nuclear import, RT, and productive infection is not clear. To study the role of capsid in the nucleus, we developed a methodology to isolate the nuclear content of HIV-1-infected cells to measure the amount of capsid (Figure 1A). This methodology consists of performing synchronized infections of human cells with HIV-1 using an MOI of 2 and fractionating cells at different time points after infection. Nuclear and cytoplasm fractions are analyzed for HIV-1 capsid by western blotting using anti-p24 antibodies. The quality of fractionation is controlled by western blotting using specific antibodies against the nuclear marker Nopp140 and the cytosolic marker GAPDH (or α-tubulin) (Figure 1A).

Because the use of the small molecules PF74 and BI-2 blocks HIV-1 infection before the production of 2-LTR circles and prevents Nup153 binding to capsid (Balasubramaniam et al., 2019; Buffone et al., 2018; Fricke et al., 2014a), we decided to test whether these

compounds had an effect on the import of capsid into the nucleus. To track the nuclear import of capsid, we utilized HIV-1$_{NL4-3}$ env viruses pseudotyped with the envelope protein of vesicular stomatitis virus G protein (VSV-G) expressing GFP as a reporter of infection (HIV-1-GFP) as described in STAR Methods. We performed synchronized infections of human A549 cells using HIV-1-GFP viruses (MOI = 2) in the presence of 10 μM PF74 or 50 μM BI-2 for 8 h. Both compounds prevented the import of HIV-1 capsid into the nucleus (Figure 1B). These results agree with findings demonstrating that PF74 and BI-2 prevent 2-LTR circle formation (Fricke et al., 2014a). PF74 inhibition of HIV-1 capsid import into the nucleus was utilized as a control for this assay.

To test the specificity of this assay, we measured capsid nuclear import of HIV-1-GFP virus bearing the capsid changes N57S and N74D that result in viral resistance to PF74 (Buffone et al., 2018; Saito et al., 2016). Although we reproducibly detected decreased nuclear import of capsid for both HIV-1-N57S and HIV-1-N74D when compared to wild-type virus, PF74 did not change the nuclear import of capsid from these viruses when compared to drug-untreated controls (Figure 1C). This demonstrated that our assay specifically measures the import of HIV-1 capsid into the nucleus and that infection correlates with capsid nuclear import.

We investigated the earliest time necessary for capsid detection in the nucleus by fractionating A549 cells infected at the indicated times using HIV-1-GFP (Figure 1D). We detected capsid in the nucleus as early as 1 h post-infection. The peak of capsid in the nucleus coincides with the peak of RT, which is 8–10 h post-infection.

Our assay biochemically demonstrated the presence of capsid in the nucleus, raising questions about the amount of total capsid present in the nucleus. Using this semiquantitative assay, capsid levels were determined by fractionating cells into total (T), nuclear (N), and cytoplasmic (C) fractions. Approximately 20%–30% of total capsid corresponded with the nuclear fraction (Figure 1E). These results suggest that the fraction of capsid imported into the nucleus corresponds to the amount of capsid that is forming HIV-1 cores in the viral particle (Briggs et al., 2003, 2004, 2006). We next tested our assay using the T cell line MOLT3. As shown in Figure S1, PF74 prevented the import of HIV-1 capsid into the nucleus of T cells.

To corroborate these biochemical findings, we performed similar infections and imaged the viral capsid using confocal microscopy in the presence of PF74. As shown in Figure S2, PF74 prevented the entry of capsid into the nucleus.

Formation of CPSF6 Speckles in the Nucleus during HIV-1 Infection Requires Intact Capsid in the Nucleus

Our investigations revealed that infection of human cells by HIV-1 triggers a change in the nuclear staining pattern of the HIV-1 cofactor CPSF6 from diffuse to speckled at 8 or 16 h post-infection when compared to mock controls. As shown in Figures 2A and 2B, infection of HeLa cells using HIV-1 viruses containing luciferase as a reporter of infection (HIV-1-Luc) at an MOI of ~2 for 8 or 16 h changed the nuclear localization of CPSF6 from diffuse to speckled. Interestingly, when using HIV-1 viruses bearing the capsid mutation N74D

(HIV-1-N74D), we did not observe the formation of speckles (Figure 2A). These experiments revealed that an intact capsid capable of binding CPSF6 triggers the formation of speckles. Visual inspection of HIV-1-induced CPSF6 nuclear speckles resembles the transcriptionally active SC35 domains (Hall et al., 2006). The pre-mRNA splicing machinery shows a punctate nuclear localization pattern that is termed a speckled pattern or SC35 domains. These discrete domains with a diameter ranging from 0.5 to 3 μm facilitate transcription of highly active genes and are visualized using antibodies against the spliceosome assembly factor SC35 (Fu and Maniatis, 1990; Hall et al., 2006). Because HIV-1 infection increases expression of SC35 by 2- to 3-fold (D'Agostino et al., 2000; Maldarelli et al., 1998), we tested whether CPSF6 speckles localized to SC35 domains. As shown in Figure 2A, CPSF6 localized to SC35 domains, which suggested the potential recruitment of viral complexes through capsid to this transcriptionally active domains.

To establish whether the presence of capsid in the nucleus triggers formation of CPSF6 speckles, we investigated the role of HIV-1 capsid nuclear import in the formation of CPSF6 speckles. HeLa cells were challenged with wild-type and mutant HIV-1 viruses in the presence of PF74 using an MOI of ~2 for 8 or 16 h. Subsequently, cells were fixed and stained for CPSF6 and capsid. As shown in Figure 2B, HIV-1 infection induced formation of CPSF6 speckles in the nuclear compartment at 8 and 16 h post-infection. By contrast, uninfected cells showed a diffuse staining pattern for CPSF6. Inhibition of capsid nuclear import with PF74 during HIV-1 infection resulted in a diffuse staining of CPSF6, suggesting that the presence of capsid in the nucleus is required for CPSF6 to converge into nuclear speckles. We next investigated whether nuclear capsid is sufficient for CPSF6 speckle formation by challenging HeLa cells with HIV-1-N74D and HIV-1-N57A viruses, which import capsid into the nucleus during infection. Although capsid protein of HIV-1-N74D and HIV-1-N57S viruses entered the nuclei (see Figure 1C), CPSF6 showed a diffuse staining pattern (Figure 2B). Overall, these experiments show that the formation of nuclear CPSF6 speckles requires the interaction of CPSF6 with capsid in the nucleus.

Assembled Capsid Complexes Are Imported into the Nuclear Compartment during HIV-1 Infection

Capsid import into the nucleus during infection may be occurring by different mechanisms; monomeric capsid is imported into the nucleus, assembled capsid complexes are imported into the nucleus, or both. To test whether assembled HIV-1 capsid complexes are imported into the nucleus, we measured nuclear capsid in human A549 and HT1080 cells expressing the restriction factors tripartite motif cyclophilin A (TRIMCyp) and rhesus TRIM5α (TRIM5α$_{rh}$), which accelerate HIV-1 uncoating in the cytoplasm of infected cells (Diaz-Griffero et al., 2007; Stremlau et al., 2006). Accelerated uncoating causes the disassembly of the core or higher-order capsid complexes. To this end, we challenged human A549 and HT1080 cells stably expressing TRIMCyp or TRIM5α$_{rh}$ with HIV-1-GFP at a MOI = 2 for 8 h. TRIMCyp and TRIM5α$_{rh}$, which potently blocked HIV-1 infection (Figures S3A and S3B), prevented HIV-1 capsid import into the nucleus (Figure 3A). These experiments demonstrate that the presence of capsid in the nucleus results from the import of larger capsid complexes, as has been shown for other viruses (Cohen et al., 2011; Fay and Panté,

2015; Whittaker et al., 2000). These larger capsid complexes may be complete cores or pieces of the core that are associated to the viral genome.

We explored whether factors that stabilize the HIV-1 core during infection affect the presence of capsid in the nucleus. Expression of myxovirus resistance B protein (MxB) or CPSF6 that contains the nuclear export signal of PKIα (NES-CPSF6) prevents uncoating by stabilizing the HIV-1 core during infection (De Iaco et al., 2013; Fricke et al., 2013, 2014b). Expression of MxB or NES-CPSF6, which potently restricts HIV-1 (Figures S3A and S3B), did not affect the ability of the HIV-1 capsid to reach the nuclear compartment (Figure 3B). These results demonstrate that stabilized HIV-1 capsid complexes, which may be intact cores or slightly uncoated cores, are imported into the nuclear compartment, in agreement with our findings suggesting that large capsid complexes or complete cores are the source of nuclear capsid.

Experiments using our nuclear import assay functionally suggested that assembled capsids are transported into the nucleus; however, western blots cannot distinguish between assembled or disassembled capsid within the nucleus. To directly test whether large assembled capsid complexes can be imported into the nucleus using an HIV-1 core resistant to disassembly, we produced an HIV-1-GFP virus with a stabilized capsid, taking advantage of the capsid mutations A14C/E45C that stabilize purified capsid hexamers *in vitro* through disulfide bridges between monomers in the hexamer (Pornillos et al., 2010; Selyutina et al., 2018). This virus lacked defects in viral budding, maturation, and RT; however, HIV-1-A14C/E45C virus was incapable of forming 2-LTR circles and productive infection (Figures S3C–S3F). In addition, the core of HIV-1-A14C/E45C virus showed greater stability when compared to wild-type in our fate of the capsid assay (Figure S3G). Human A549 cells were challenged using HIV-1-A14C/E45C virus, and nuclear fractions were isolated 8 h post-infection. To distinguish assembled from disassembled capsid, the nuclear fractions were analyzed in the presence or absence of the reducing agent β-mercaptoethanol. Remarkably, most of the HIV-1-A14C/E45C capsid in the nuclear fraction was in the assembled form, since its migration by SDS-PAGE was sensitive to β-mercaptoethanol (Figures 3C and S4). These results illustrate that large, assembled capsid complexes are imported into the nucleus. Additionally, nuclear import of HIV-1-A14C/E45C capsid was not sensitive to PF74, which may be due to the enhanced stability of HIV-1-A14C/E45C cores. This corresponds with our earlier findings inferring that the observed nuclear capsids are the result of importing assembled capsid complexes and/or complete cores.

RT Inhibition Does Not Affect Nuclear Capsid Levels during HIV-1 Infection

Previous evidence has shown that inhibition of RT enhances HIV-1 core stability (Hulme et al., 2011; Yang et al., 2013). Furthermore, acceleration of uncoating correlates with inhibition of RT, suggesting that RT occurs before or during uncoating (Arfi et al., 2009; Roa et al., 2012). Given these observations, we decided to test whether inhibiting RT affects nuclear import by infecting human A549 cells with HIV-1 in the presence of the RT inhibitors nevirapine and azidothymidine (AZT). Inhibition of RT did not affect capsid import into the nucleus during infection (Figure 4A). Similar results were obtained when using HIV-1-GFP virus bearing the mutation D185N in the reverse transcriptase enzyme that

genetically ablates RT (Yang et al., 2013) (Figure 4A). This is in agreement with the notion that large assembled capsid complexes are imported into the nucleus while RT is occurring.

To evaluate the functionality of the nuclear HIV-1 capsid during RT inhibition, we monitored the formation of CPSF6 speckles by challenging HeLa cells with HIV-1 in the presence of AZT for 8 and 16 h. As shown in Figure 4B, infection in the presence of AZT resulted in the formation of CPSF6 speckles, showing that nuclear capsid is functional in the presence of RT inhibitors.

Next, we measured nuclear import of HIV-1 capsid in cells expressing the restriction factor SAMHD1, which is nuclear and inhibits RT (Hrecka et al., 2011; Laguette et al., 2011). To this end, we challenged non-cycling human U937 °Cells stably expressing SAMHD1 with HIV-1-GFP at an MOI of 2 for 8 h. Non-cycling cells are obtained by treating cycling U937 °Cells with phorbol 12-myristate 13-acetate (PMA) for 24 h (Schwende et al., 1996). Although SAMHD1 blocked HIV-1-GFP infection before RT (Figure S5), cellular fractionation revealed that expression of SAMHD1 does not affect the entry of capsid into the nucleus (Figure 4C). In agreement, inhibition of RT by SAMHD1 does not affect the nuclear import of HIV-1 capsid in non-cycling cells.

HIV-1 RT Occurs in the Nuclear Compartment

Our results have indicated that large assembled capsid complexes can enter the nuclear compartment even during RT inhibition, supporting the hypothesis that RT occurs in the nuclear compartment. To further validate these observations, human A549 and dog Cf2Th cells were challenged with HIV-1-GFP virus for 2, 4, and 8 h. Subsequently, cells were fractionated, and 10% aliquots of each fraction (total, cytoplasm, and nuclear) were analyzed for capsid protein content using western blotting (Figures 5A, 5B, S6, and S7) and monitored for RT using real-time PCR (to detect early products, minus-strand transfer, intermediate products, and late reverse-transcribed products) (Figures 5A, 5B, S6, and S7). As controls, the RT inhibitor nevirapine and mock-infected cells were utilized. All RT intermediates tested were enriched in the nucleus when compared to the cytosolic fraction. These results showed that most of HIV-1 RT is found in the nucleus.

DISCUSSION

Our biochemical assay to measure the amount of nuclear HIV-1 capsid during infection is based on separating HIV-1-infected cells into nuclear and cytosolic fractions. We found that the amount of nuclear capsid peaks at 8–10 h post-infection in synchronized infections, which coincides with the peak of late RT. As a control, we used the small molecules PF74 and BI-2 that prevent 2-LTR circle formation measured by real-time PCR (Balasubramaniam et al., 2019; Fricke et al., 2014a). The absence of 2-LTR circles during HIV-1 infection is usually interpreted as a block to nuclear import, but the block may be at any step before 2-LTR circle formation, which occurs in the nucleus (Butler et al., 2001). Accordingly, we discovered that PF74 and BI-2 prevented capsid entry into the nucleus. Treatment with PF74 during infection with HIV-1 virus bearing the capsid changes N57S and N74D did not prevent capsid nuclear import, which agrees with the fact that these viruses are resistant to

PF74 (Buffone et al., 2018; Saito et al., 2016). Besides a specificity control, the infectivity of these mutant viruses correlates nuclear capsid with productive infection.

Our experiments herein show that CPSF6 forms nuclear speckles upon HIV-1 infection. Interestingly, we demonstrate that CPSF6 speckles only form when CPSF6 binds to capsid and when capsid is physically in the nucleus. Intriguingly, CPSF6 nuclear speckles localized to SC35 domains, which are transcriptionally active domains (Hall et al., 2006). A possible scenario is that CPSF6 through its interaction with capsid recruits viral complexes to transcriptionally active sites for viral RT, integration, and/or expression.

Nuclear capsid raised the question of how capsid reaches the nuclear compartment. We considered that capsid might be reaching the nucleus in two different oligomeric states: assembled and/or disassembled. To this end, we took advantage of the ability of TRIM5α_{rh} and TRIMCyp to disassemble the HIV-1 core in the cytoplasm of infected cells (Diaz-Griffero et al., 2007; Stremlau et al., 2006). Our experiments revealed that HIV-1 capsid does not reach the nuclear compartment of cells stably expressing TRIM5α_{rh} or TRIMCyp, implying that assembled capsid is necessary to enter the nucleus. One possibility is that successful nuclear import of the HIV-1 replication complex depends upon its association with assembled capsid, which may not be a complete core but needs to be a substantial structure. In agreement, Zila and colleagues showed that the relative amount of capsid protein in post-fusion complexes remained stable until reaching the nucleus (Zila et al., 2019). The entry of assembled capsid into the nucleus is not novel, since other viruses import complete cores into the nucleus (Fay and Panté, 2015). Therefore, it is not unlikely that HIV-1 uses a similar nuclear import strategy. By contrast, we found that the HIV-1 capsid reaches the nuclear compartment of cells stably expressing MxB or NES-CPSF6, which are proteins that prevent HIV-1 uncoating (De Iaco et al., 2013; Fricke et al., 2013, 2014b). This led us to conclude that factors that stabilize the HIV-1 core did not prevent nuclear import of capsid, strengthening the notion that nuclear capsid is the result of importing assembled HIV-1 capsid.

To further understand whether assembled capsid enters the nuclear compartment, we took advantage of the capsid changes A14C/E45C, which result in the formation of disulfide bonds between capsid monomers that stabilize the HIV-1 core. Interestingly, we found that the electrophoretic migration for most of the HIV-1 capsid found in the nucleus is sensitive to reducing agent, implying that most of the capsid found in the nucleus is assembled strengthening the notion that assembled capsid enters the nucleus.

Several lines of evidence suggest that HIV-1 RT occurs before or during uncoating (Arfi et al., 2009; Hulme et al., 2011; Roa et al., 2012; Stremlau et al., 2006; Yang et al., 2013), which is defined as dissociation of monomeric capsids from the core. Therefore, we decided to test whether inhibiting RT modulates capsid import into the nucleus. We observed that inhibition of RT does not change the amount of capsid reaching the nucleus when compared to wild-type virus. Accordingly, we observed that the RT block imposed by SAMHD1 to HIV-1 does not prevent capsid transport into the nucleus. Because SAMHD1 is a nuclear protein, it is likely that RT is inhibited in the nucleus, suggesting that RT is occurring in the nuclear compartment.

Our studies showed that assembled capsid reaches the nucleus; therefore, it is reasonable to think that the RT process occurs in the nucleus. To this end, we measured the different steps of RT in nuclear and cytosolic fractions over time. This revealed that the nuclear fraction was enriched on RT intermediates when compared to the cytosolic fraction. Although the conventional view is that RT occurs in the cytoplasm followed by the transport of the complete viral DNA into the nucleus, we show that most of the RT intermediates are found in the nucleus. Though the nuclear fraction is enriched in RT intermediates when compared to cytosol, we detected a small but significant amount of late reverse transcripts in cytosolic fractions, indicating that RT can be initiated and completed in the cytosol.

Conceptually, the occurrence of RT in the nucleus will be more efficient for the virus, since integration also occurs in the nucleus. While this manuscript was under review, Burdick and colleagues found that RT is occurring in the nuclear compartment by tracking single viral particles using fluorescent microscopy (Burdick et al., 2020).

Combination of our results with the work of others suggests a model in which the HIV-1 core enters the cytoplasm to begin a slow uncoating process. At the same time, it is likely that the viral complexes initiate RT. Although the HIV-1 replication complex slowly loses capsid monomers, it has to reach the nuclear pore containing a substantial amount of the assembled capsid to gain access to the nucleus. While RT likely begins in the cytoplasm, our results indicate that most of the RT intermediates are found in the nuclear compartment, which is in stark contrast to the common notion that RT and uncoating occurs in the cytosol. As most of the RT occurs in the nucleus and RT occurs before or during uncoating, our findings indicate that uncoating also occurs in the nucleus. These results fundamentally change our understanding of HIV-1 infection and conclude that nuclear import precedes RT and uncoating.

STAR★METHODS

RESOURCE AVAILABILITY

Lead Contact—Further information and requests for resources and reagents should be directed to and will be fulfilled by the Lead Contact, Felipe Diaz-Griffero (Felipe.Diaz-Griffero@einsteinmed.org)

Materials Availability—This study generated the following new plasmids: HIV-1-N57S, HIV-1-N74D, HIV-1-D185N, HIV-1-A14C/E45C. Plasmids generated in this study are available upon request. Further information and requests for plasmids, resources, and reagents should be directed to and will be fulfilled by the lead contact Felipe Diaz-Griffero (Felipe.Diaz-Griffero@einsteinmed.org)

Data and Code Availability—This study did not generate any unique datasets or code.

EXPERIMENTAL MODEL AND SUBJECT DETAILS

Bacterial strains—All molecular cloning was carried out in *E. coli* DH5α competent cells. This bacterial stain was routinely grown in Luria-Bertani (LB) medium at 37 °C while shaking at 200 RPM.

Human cell lines—Human MOLT3 T lymphoblast cells obtained from the American type culture collection (ATCC) were grown at 37°C in Roswell Park Memorial Institute (RPMI) medium supplemented with 10% fetal bovine serum (FBS) and 1% penicillin-streptomycin. Human 293T/17, A549, HeLa, and HT1080, and canine Cf2Th (ATCC) cells were grown at 37°C in Dulbecco's modified eagle medium (DMEM) supplemented with 10% FBS and 1% penicillin-streptomycin.

METHOD DETAILS

Subcellular fractionation to detect HIV-1 capsid in the nucleus—The specified mammalian cells (5×10^6 cells) were challenged with HIV-1 viruses at a MOI = 2 for the indicated times. Cells were harvested using trypsin for 2–5 minutes at 37 °C. Harvested cells were washed twice with $1 \times$ cold PBS by centrifugation at 2000 rpm for 7 min at 37 °C. Supernatant was discarded and cell pellet was resuspended in 1 mL of PBS. 1/10 aliquot of the cell suspension (100 μL) was centrifuged (2000 rpm for 7 minutes at 37 °C), supernatant was discarded and cell pellet was resuspended in 35 μL of WCE (50 mM Tris pH = 8.0, 280 mM NaCl, 10% glycerol, 0.5% NP-40, 5 mM $MgCl_2$, 250 units/mL Benzonase, $1 \times$ protease inhibitor), incubated for 1 hour on ice, centrifuged at 13400 rpm for 1 hour at 37 °C, then resulting supernatant was mixed with $5 \times$ Laemmli buffer and used to measure the *total* amount of capsid. The rest of the cell suspension (900 μL) was centrifuged (2000 rpm for 7 min at 37 °C), supernatant was discarded and cell pellet was resuspended in 315 μL of lysis buffer (10 mM Tris pH = 6.8, 1 mM DTT, 1 mM $MgCl_2$, 10% sucrose, 100 mM NaCl, 0.5% NP-40, $1 \times$ protease inhibitor) and incubated for 5 min on ice. Subsequently, the sample was centrifuged at 2500 rpm for 2 min at 37 °C. The resulting supernatant and pellet correspond to *cytosolic* and *nuclear* fractions, respectively. Next, 1/9 aliquot of supernatant (35 μL) was mixed with $5 \times$ Laemmli buffer and used as *cytosolic* fraction. The nuclear pellet was washed twice using 1 mL of lysis buffer without NP-40 (10 mM Tris, pH = 6.8, 1 mM DTT, 1 mM $MgCl_2$, 10% sucrose, 100 mM NaCl, $1 \times$ protease inhibitor) by gently inverting the tube 2–3 times. The sample was then centrifuged at 2500 rpm for 2 min at 37 °C, and the supernatant was discarded. The nuclear pellet was resuspended in 315 μL of extraction buffer (10 mM Tris, pH = 6.8, 1 mM DTT, 1 mM $MgCl_2$, 10% sucrose, 400 mM NaCl, $1 \times$ protease inhibitor), and incubated on ice for 10 min. Subsequently, the sample was centrifuged at 7000 rpm for 2 min at 37 °C. 1/9 aliquot of the supernatant (35 μL) was mixed with $5 \times$ Laemmli buffer and used as *nuclear* fraction. Proportional amounts of *total*, *cytosolic*, and *nuclear* fractions were analyzed by western blot using anti-p24, anti-Nopp140, anti-α-tubulin, or anti-GAPDH antibodies detailed below.

Fate of the capsid assay—Human A549 cells were infected with p24-normalized amounts of wild-type HIV-1-GFP or mutant HIV-1-A14C/E45C-GFP viruses in the presence of 10 μM PF74 or DMSO as vehicle control. After incubation at 37 °C for 12 hours, cells were detached with 7 mg/mL Pronase for 5 minutes on ice and washed 3 times with ice-cold PBS. Cell pellets were resuspended in hypotonic buffer (10 mM Tris-HCl, pH 8.0; 10 mM KCl; 1 mM EDTA) and incubated for 20 minutes on ice. Cells were lysed in a 7.0 mL Dounce homogenizer with pestle B. Cellular debris and nuclear fraction were removed by centrifugation for 7 minutes at 3000 rpm. The supernatant fraction was layered onto a 50% sucrose (weight:volume) cushion in 1x PBS and centrifuged at 125,000 x g for 2 hours at 37

°C in a Beckman SW41 rotor. Input, soluble, and pellet fractions were analyzed by western blotting using anti-p24 antibody.

Creation of stable cell lines expressing different proteins—Retroviral vectors encoding rhesus TRIM5α$_{rh}$, owl monkey TRIMCyp (Diaz-Griffero et al., 2006; Stremlau et al., 2006), human CPSF6(1–358) (Fricke et al., 2013), or human MxB proteins were created using the pLPCX vector (Fricke et al., 2014b). The different proteins were tagged with an influenza hemagglutinin (HA) or FLAG epitope tag at the C terminus. Recombinant viruses were produced in 293T cells by co-transfecting pLPCX plasmids with pVPack-GP and pVPack-VSV-G packaging plasmids (Stratagene). The pVPack-VSV-G plasmid encodes the vesicular stomatitis virus (VSV) G envelope glycoprotein, which allows efficient entry into a wide range of vertebrate cells. The indicated mammalian cells were transduced and selected in the appropriate concentration of puromycin (1–5 μg/mL).

Production of HIV-1-GFP viruses—Recombinant HIV-1 expressing GFP (HIV-1-GFP) were prepared as previously described (Diaz-Griffero et al., 2008). Briefly, HIV-1-GFP viruses are produced by co-transfecting HIV-1$_{NL4-3}$ env, LTR-GFP-LTR, and the envelope of vesicular stomatitis virus (VSV-G). For infections, 3×10^4 human cells seeded in 24-well plates were incubated at 37 °C with virus for 24 h. Cells were washed and returned to culture for 48 h, then subjected to flow cytometric analysis with a FACScan (Becton Dickinson). HIV-1 viral stocks were titrated by serial dilution on susceptible cells to determine the infectivity of viruses.

Immunofluorescense Microscopy and Image quantification—Human HeLa cells were attached to poly-L-Lysine–coated chamber slides (BD Biosciences) and regular chamber slides (Nalgene Nunc), respectively. After HIV-1 infections and/or drug treatments, chamber slides were rinsed with PBS and fixed with 4% Paraformaldehyde (Boston Bioproducts) in PBS. Subsequently, cells were permeabilized using 0.1% Triton X-100 for 5 min at room temperature. Non-specific binding was prevented using blocking solution (3% bovine serum albumin in PBS) for 30 min at room temperature. To stain for the different proteins, samples were incubated with primary antibodies in blocking solution (anti-human CPSF6, Novus; anti-HIV-1-capsid-71–31, AIDS Reagent Repository; anti-SC-35, Sigma-Aldrich; anti-HA, Novus). After unbound antibodies were removed by washing with PBS, cells were incubated with appropriate secondary antibodies against mouse, rabbit, goat or human in blocking solution. Chamber slides were mounted using Gel Mount (Biomedia) containing an anti-fade reagent. Dried chamber slides were imaged using a Deltavision epifluorescent microscope system fitted with an automated stage (Applied Precision, Inc) and images were captured in z series on a CCD digital camera using a 63X lens. Out-of-focus images were digitally removed using the Softworks deconvolution software (Applied Precision, Inc). The number cells containing CPSF6 nuclear speckles was determined by visual inspection of 200 cells per sample for 3 independent experiments.

Quantitative PCR to detect reverse transcription intermediates—Total DNA was extracted from 10% aliquots of each fraction (*total*, *cytosolic*, and *nuclear*, obtained during subcellular fractionation at 2 h, 4 h, and 8 h post-infection) using the QIAamp DNA micro

kit (QIAGEN). As a parallel control, another 10% aliquot of the same fractions were analyzed by western blotting using anti-p24, anti-Nopp 140, and anti-α-tubulin antibodies. Viral DNA forms of HIV-1 were amplified using real-time PCR. Reactions were performed in $1 \times$ TaqMan Universal Probe Master Mix II, with UNG $2 \times$ (Thermo Fischer Scientific) in 20 μL volume. The reaction consisted of the following steps: initial denaturation (95 °C for 15 min), 40 cycles of amplification (95 °C for 15 s, 58 °C for 30 s, 72 °C for 30 s). Primer or probe sequences are as follows: early products: hRU5-F2: 5′-GCCTCAATAAAGCTTGCCTTGA-3′; hRU5-R: 5′-TGACTAAAAGGGTCTGAGGGATCT-3′; hRU5-P: 5′-(FAM)-AGAGTCACACAACAG ACGGGCACACACTA-(TAMRA)-3′; minus strand transfer: FST-F1: 5′-GAGCCCTCAGATGCTGCATAT-3′, SS-R4: 5′-CCACACTGAC TAAAAGGGTCTGAG-3′, P-HUS-SS1: 5′-(FAM)-TAGTGTGTGCCCGTCTGTTGTGTGAC-(TAMRA)-3′; intermediate products: GagF1: 5′-CTAGAACGATTCGCAGTTAATCCT-3′, GagR1: 5′-CTATCCTTTGATGCACACAATAGAG-3′, P-HUS-103: 5′-(FAM)-CAT CAGAAGGCTGTAGACAAATACTGGGA-(TAMRA)-3′; late products: MH531: 5′-TGTGTGCCCGTCTGTTGTGT-3′; MH532: 5′-GAGTCCTGCGTCGAGAGATC-3′; LRT-P: 5′-(FAM)-CAGTGGCGCCCGAACAGGGA-(TAMRA)-3′.

Western blot analysis—Proteins were detected by western blot using anti-p24 (1:1,000 dilution, #3637, NIH), anti-Nopp 140 (1:5,000 dilution, a generous gift from U. Thomas Meier, Albert Einstein College of Medicine), anti-α-tubulin (1:8,000 dilution, #PA5–29444, Invitrogen), anti-FLAG (1:1,000 dilution, Sigma), anti-hemagglutinin (HA) (1:1,000 dilution, Sigma), and anti-glyceraldehyde-3-phosphate dehydrogenase (GAPDH) (1:5,000 dilution, Invitrogen). Secondary antibodies against rabbit and mouse IgG conjugated to IRDye 680LT or IRDye 800CW were obtained from Li-Cor (1:10,000 dilution). Bands were detected by scanning blots using the Li-Cor Odyssey imaging system in the 700 nm or 800 nm channels.

QUANTIFICATION AND STATISTICAL ANALYSIS

Quantification of the intensity of western blot bands was performed using ImageJ. The mean and standard deviation values were calculated using GraphPad Prism 7.0c. Statistical analysis was performed using unpaired t test.

Supplementary Material

Refer to Web version on PubMed Central for supplementary material.

ACKNOWLEDGMENTS

REFERENCES

Arfi V, Lienard J, Nguyen XN, Berger G, Rigal D, Darlix JL, and Cimarelli A. (2009). Characterization of the behavior of functional viral genomes during the early steps of human immunodeficiency virus type 1 infection. J. Virol. 83, 7524–7535. [PubMed: 19457995]

Balasubramaniam M, Zhou J, Addai A, Martinez P, Pandhare J, Aiken C, and Dash C. (2019). PF74 inhibits HIV-1 integration by altering the composition of the preintegration complex. J. Virol. 93, e01741–18.

Bejarano DA, Peng K, Laketa V, Börner K, Jost KL, Lucic B, Glass B, Lusic M, Müller B, and Kräusslich HG (2019). HIV-1 nuclear import in macrophages is regulated by CPSF6-capsid interactions at the nuclear pore complex. eLife 8, e41800.

Briggs JA, Wilk T, Welker R, Kräusslich HG, and Fuller SD (2003). Structural organization of authentic, mature HIV-1 virions and cores. EMBO J. 22, 1707–1715. [PubMed: 12660176]

Briggs JA, Simon MN, Gross I, Kräusslich HG, Fuller SD, Vogt VM, and Johnson MC (2004). The stoichiometry of Gag protein in HIV-1. Nat. Struct. Mol. Biol. 11, 672–675. [PubMed: 15208690]

Briggs JA, Grünewald K, Glass B, Förster F, Kräusslich HG, and Fuller SD (2006). The mechanism of HIV-1 core assembly: insights from three-dimensional reconstructions of authentic virions. Structure 14, 15–20. [PubMed: 16407061]

Buffone C, Martinez-Lopez A, Fricke T, Opp S, Severgnini M, Cifola I, Petiti L, Frabetti S, Skorupka K, Zadrozny KK, et al. (2018). Nup153 unlocks the nuclear pore complex for HIV-1 nuclear translocation in nondividing cells. J. Virol. 92, e00648–18.

Burdick RC, Delviks-Frankenberry KA, Chen J, Janaka SK, Sastri J, Hu WS, and Pathak VK (2017). Dynamics and regulation of nuclear import and nuclear movements of HIV-1 complexes. PLoS Pathog. 13, e1006570.

Burdick RC, Li C, Munshi M, Rawson JMO, Nagashima K, Hu WS, and Pathak VK (2020). HIV-1 uncoats in the nucleus near sites of integration. Proc. Natl. Acad. Sci. USA 117, 5486–5493. [PubMed: 32094182]

Butler SL, Hansen MS, and Bushman FD (2001). A quantitative assay for HIV DNA integration in vivo. Nat. Med. 7, 631–634. [PubMed: 11329067]

Chin CR, Perreira JM, Savidis G, Portmann JM, Aker AM, Feeley EM, Smith MC, and Brass AL (2015). Direct visualization of HIV-1 replication intermediates shows that capsid and CPSF6 modulate HIV-1 intra-nuclear invasion and integration. Cell Rep. 13, 1717–1731. [PubMed: 26586435]

Cohen S, Au S, and Panté N. (2011). How viruses access the nucleus. Biochim. Biophys. Acta 1813, 1634–1645. [PubMed: 21167871]

D'Agostino DM, Ferro T, Zotti L, Meggio F, Pinna LA, Chieco-Bianchi L, and Ciminale V. (2000). Identification of a domain in human immunodeficiency virus type 1 rev that is required for functional activity and modulates association with subnuclear compartments containing splicing factor SC35. J. Virol. 74, 11899–11910. [PubMed: 11090190]

De Iaco A, Santoni F, Vannier A, Guipponi M, Antonarakis S, and Luban J. (2013). TNPO3 protects HIV-1 replication from CPSF6-mediated capsid stabilization in the host cell cytoplasm. Retrovirology 10, 20. [PubMed: 23414560]

Diaz-Griffero F, Vandegraaff N, Li Y, McGee-Estrada K, Stremlau M, Welikala S, Si Z, Engelman A, and Sodroski J. (2006). Requirements for capsid-binding and an effector function in TRIMCyp-mediated restriction of HIV-1. Virology 351, 404–419. [PubMed: 16650449]

Diaz-Griffero F, Kar A, Lee M, Stremlau M, Poeschla E, and Sodroski J. (2007). Comparative requirements for the restriction of retrovirus infection by TRIM5alpha and TRIMCyp. Virology 369, 400–410. [PubMed: 17920096]

Diaz-Griffero F, Perron M, McGee-Estrada K, Hanna R, Maillard PV, Trono D, and Sodroski J. (2008). A human TRIM5alpha B30.2/SPRY domain mutant gains the ability to restrict and prematurely uncoat B-tropic murine leukemia virus. Virology 378, 233–242. [PubMed: 18586294]

Fay N, and Panté N. (2015). Nuclear entry of DNA viruses. Front. Microbiol. 6, 467. [PubMed: 26029198]

Francis AC, and Melikyan GB (2018). Single HIV-1 imaging reveals progression of infection through CA-dependent steps of docking at the nuclear pore, uncoating, and nuclear transport. Cell Host Microbe 23, 536–548.e536.

Fricke T, Valle-Casuso JC, White TE, Brandariz-Nuñez A, Bosche WJ, Reszka N, Gorelick R, and Diaz-Griffero F. (2013). The ability of TNPO3-depleted cells to inhibit HIV-1 infection requires CPSF6. Retrovirology 10, 46. [PubMed: 23622145]

Fricke T, Buffone C, Opp S, Valle-Casuso J, and Diaz-Griffero F. (2014a). BI-2 destabilizes HIV-1 cores during infection and prevents binding of CPSF6 to the HIV-1 capsid. Retrovirology 11, 120. [PubMed: 25496772]

Fricke T, White TE, Schulte B, de Souza Aranha Vieira DA, Dharan A, Campbell EM, Brandariz-Nuñez A, and Diaz-Griffero F. (2014b). MxB binds to the HIV-1 core and prevents the uncoating process of HIV-1. Retrovirology 11, 68. [PubMed: 25123063]

Fu XD, and Maniatis T. (1990). Factor required for mammalian spliceosome assembly is localized to discrete regions in the nucleus. Nature 1, 437–441.

Hall LL, Smith KP, Byron M, and Lawrence JB (2006). Molecular anatomy of a speckle. Anat. Rec. A Discov. Mol. Cell. Evol. Biol. 288, 664–675. [PubMed: 16761280]

Hrecka K, Hao C, Gierszewska M, Swanson SK, Kesik-Brodacka M, Srivastava S, Florens L, Washburn MP, and Skowronski J. (2011). Vpx relieves inhibition of HIV-1 infection of macrophages mediated by the SAMHD1 protein. Nature 474, 658–661. [PubMed: 21720370]

Hulme AE, Perez O, and Hope TJ (2011). Complementary assays reveal a relationship between HIV-1 uncoating and reverse transcription. Proc. Natl. Acad. Sci. USA 108, 9975–9980. [PubMed: 21628558]

Hulme AE, Kelley Z, Foley D, and Hope TJ (2015). Complementary assays reveal a low level of CA associated with viral complexes in the nuclei of HIV-1-infected cells. J. Virol. 89, 5350–5361. [PubMed: 25741002]

Katz RA, Greger JG, and Skalka AM (2005). Effects of cell cycle status on early events in retroviral replication. J. Cell. Biochem. 94, 880–889. [PubMed: 15669021]

Kittur N, Zapantis G, Aubuchon M, Santoro N, Bazett-Jones DP, and Meier UT (2007). The nucleolar channel system of human endometrium is related to endoplasmic reticulum and R-rings. Mol. Biol. Cell 18, 2296–2304. [PubMed: 17429075]

Laguette N, Sobhian B, Casartelli N, Ringeard M, Chable-Bessia C, Ségéral E, Yatim A, Emiliani S, Schwartz O, and Benkirane M. (2011). SAMHD1 is the dendritic- and myeloid-cell-specific HIV-1 restriction factor counteracted by Vpx. Nature 474, 654–657. [PubMed: 21613998]

Lewis P, Hensel M, and Emerman M. (1992). Human immunodeficiency virus infection of cells arrested in the cell cycle. EMBO J. 11, 3053–3058. [PubMed: 1322294]

Maldarelli F, Xiang C, Chamoun G, and Zeichner SL (1998). The expression of the essential nuclear splicing factor SC35 is altered by human immunodeficiency virus infection. Virus Res. 53, 39–51. [PubMed: 9617768]

Mbisa JL, Delviks-Frankenberry KA, Thomas JA, Gorelick RJ, and Pathak VK (2009). Real-time PCR analysis of HIV-1 replication post-entry events. Methods Mol. Biol. 485, 55–72. [PubMed: 19020818]

Peng K, Muranyi W, Glass B, Laketa V, Yant SR, Tsai L, Cihlar T, Müller B, and Kräusslich HG (2014). Quantitative microscopy of functional HIV post-entry complexes reveals association of replication with the viral capsid. eLife 3, e04114.

Pornillos O, Ganser-Pornillos BK, Banumathi S, Hua Y, and Yeager M. (2010). Disulfide bond stabilization of the hexameric capsomer of human immunodeficiency virus. J. Mol. Biol. 401, 985–995. [PubMed: 20600115]

Roa A, Hayashi F, Yang Y, Lienlaf M, Zhou J, Shi J, Watanabe S, Kigawa T, Yokoyama S, Aiken C, and Diaz-Griffero F. (2012). RING domain mutations uncouple TRIM5a restriction of HIV-1 from inhibition of reverse transcription and acceleration of uncoating. J. Virol. 86, 1717–1727. [PubMed: 22114335]

Rubin H, and Temin HM (1959). A radiological study of cell-virus interaction in the Rous sarcoma. Virology 7, 75–91. [PubMed: 13636057]

Saito A, Ferhadian D, Sowd GA, Serrao E, Shi J, Halambage UD, Teng S, Soto J, Siddiqui MA, Engelman AN, et al. (2016). Roles of capsid-interacting host factors in multimodal inhibition of HIV-1 by PF74. J. Virol. 90, 5808–5823. [PubMed: 27076642]

Schwende H, Fitzke E, Ambs P, and Dieter P. (1996). Differences in the state of differentiation of THP-1 cells induced by phorbol ester and 1,25-dihydroxyvitamin D3. J. Leukoc. Biol. 59, 555–561. [PubMed: 8613704]

Selyutina A, Bulnes-Ramos A, and Diaz-Griffero F. (2018). Binding of host factors to stabilized HIV-1 capsid tubes. Virology 523, 1–5. [PubMed: 30056211]

Selyutina A, Persaud M, Simons LM, Bulnes-Ramos A, Buffone C, Martinez-Lopez A, Scoca V, Di Nunzio F, Hiatt J, Marson A, et al. (2020). Cyclophilin A prevents HIV-1 restriction in lymphocytes by blocking human TRIM5alpha binding to the viral core. Cell Rep. 30, 3766–3777.e3766.

Stremlau M, Perron M, Lee M, Li Y, Song B, Javanbakht H, Diaz-Griffero F, Anderson DJ, Sundquist WI, and Sodroski J. (2006). Specific recognition and accelerated uncoating of retroviral capsids by the TRIM5alpha restriction factor. Proc. Natl. Acad. Sci. USA 103, 5514–5519. [PubMed: 16540544]

Suzuki Y, and Craigie R. (2007). The road to chromatin: nuclear entry of retroviruses. Nat. Rev. Microbiol. 5, 187–196. [PubMed: 17304248]

Temin HM, and Rubin H. (1959). A kinetic study of infection of chick embryo cells in vitro by Rous sarcoma virus. Virology 8, 209–222. [PubMed: 13669338]

Whittaker GR, Kann M, and Helenius A. (2000). Viral entry into the nucleus. Annu. Rev. Cell Dev. Biol. 16, 627–651. [PubMed: 11031249]

Yamashita M, and Emerman M. (2004). Capsid is a dominant determinant of retrovirus infectivity in nondividing cells. J. Virol. 78, 5670–5678. [PubMed: 15140964]

Yamashita M, and Emerman M. (2005). The cell cycle independence of HIV infections is not determined by known karyophilic viral elements. PLoS Pathog. 1, e18.

Yamashita M, and Emerman M. (2006). Retroviral infection of non-dividing cells: old and new perspectives. Virology 344, 88–93. [PubMed: 16364740]

Yamashita M, Perez O, Hope TJ, and Emerman M. (2007). Evidence for direct involvement of the capsid protein in HIV infection of nondividing cells. PLoS Pathog. 3, 1502–1510. [PubMed: 17967060]

Yang Y, Fricke T, and Diaz-Griffero F. (2013). Inhibition of reverse transcriptase activity increases stability of the HIV-1 core. J. Virol. 87, 683–687. [PubMed: 23077298]

Zila V, Müller TG, Laketa V, Müller B, and Kräusslich HG (2019). Analysis of CA content and CPSF6 dependence of early HIV-1 replication complexes in SupT1-R5 cells. MBio 10, e02501-19.

Highlights

- Complete or slightly uncoated HIV-1 cores are imported into the nucleus

- HIV-1 uncoating and reverse transcription occurs in the nucleus

- CPSF6 recruits HIV-1 cores to SC35 nuclear speckles for reverse transcription
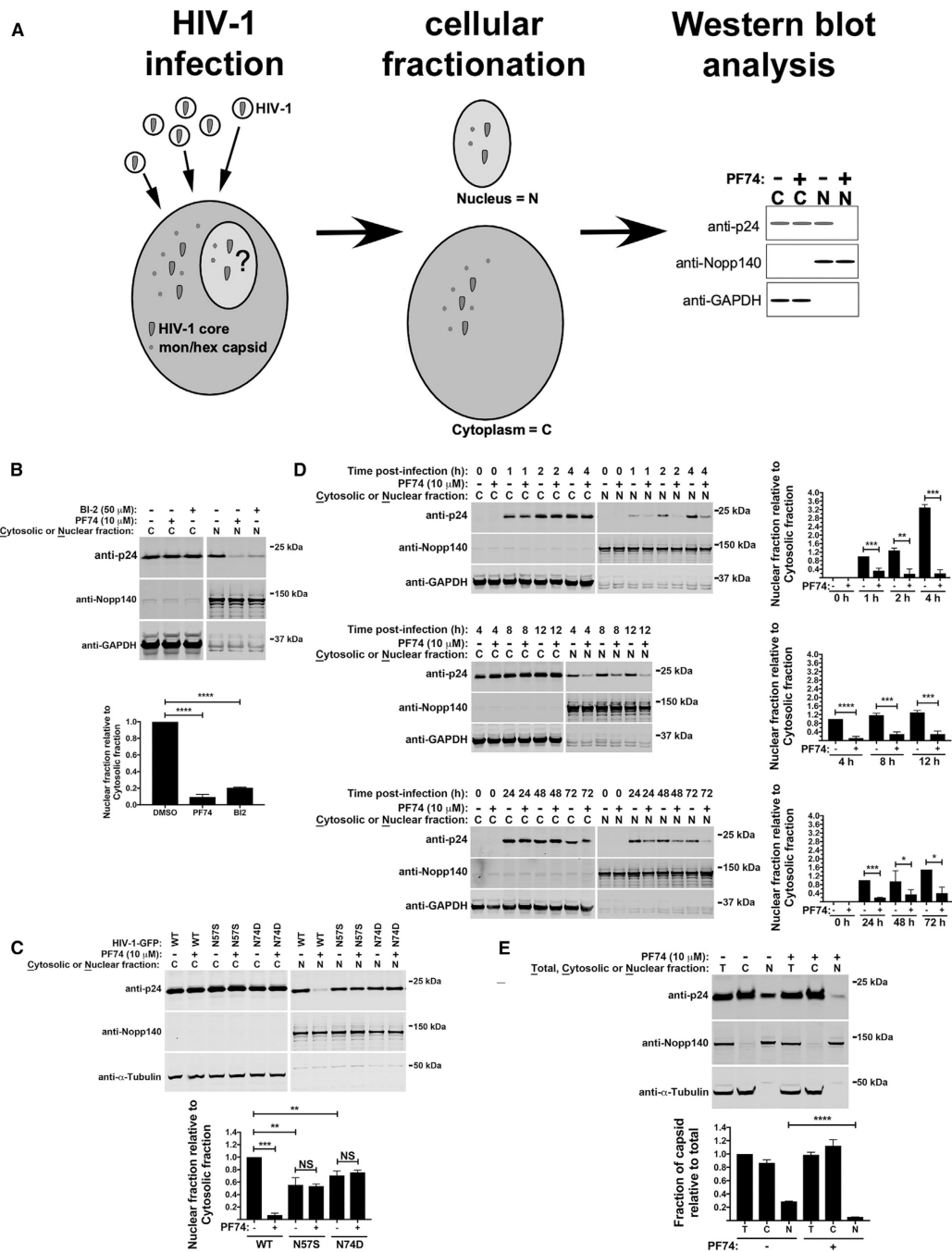
Figure 1. Biochemical Assay to Detect Capsid in the Nucleus during HIV-1 Infection

(A) Schematic representation of subcellular fractionation. Human cells infected with HIV-1 in the presence of PF74 are separated into cytosolic and nuclear fractions. PF74 prevents the nuclear import of capsid. Subsequently, fractions are analyzed by western blotting using anti-p24 antibodies. To verify the origin/purity of cellular fractions, western blotting was performed using anti-Nopp140 and anti-GAPDH/anti-tubulin antibodies, which are nuclear and cytosolic markers, respectively.

(B) Treatment with PF74 or BI-2 prevents capsid import into the nucleus. A549 cells were infected with HIV-1-GFP at an MOI of 2 for 8 h in the presence of 10 μM PF74, 50 μM BI-2, or DMSO as a vehicle control. Subsequently, cells were separated into nuclear and cytosolic fractions and analyzed for capsid content by western blotting using anti-p24 antibodies.

(C) PF74 does not affect capsid nuclear import by mutant HIV-1-N57S-GFP and HIV-1-N74D-GFP viruses. A549 cells were infected with p24-normalized HIV-1-GFP, HIV-1-N57S-GFP, or HIV-1-N74D-GFP viruses in the presence of 10 μM PF74 for 8 h. Cells were then separated into nuclear and cytosolic fractions and analyzed for capsid content by western blotting using anti-p24 antibodies.

(D) Nuclear import of capsid during infection. A549 cells were infected with HIV-1-GFP at an MOI of 2 in the presence of 10 μM PF74. At the indicated times, cells were separated into nuclear and cytosolic fractions and analyzed for capsid content by western blotting using anti-p24 antibodies. The ratio of nuclear to cytosolic capsid for three independent experiments with standard deviations is shown.

(E) Relative amounts of capsid protein in total (T), cytosolic (C), and nuclear (N) fractions. A549 cells were infected with HIV-1-GFP at a MOI = 2 in the presence of 10 μM PF74 for 8 h. Cells were separated into nuclear and cytosolic fractions. Total, cytosolic, and nuclear fractions were analyzed by western blotting using anti-p24, anti-Nopp140, and anti-GAPDH antibodies. The amount of capsid relative to the total for three independent experiments with standard deviations is shown.

$*p < 0.005$; $**p < 0.001$; $***p < 0.0005$; $****p < 0.0001$; NS, not significant (as determined by an unpaired t test).
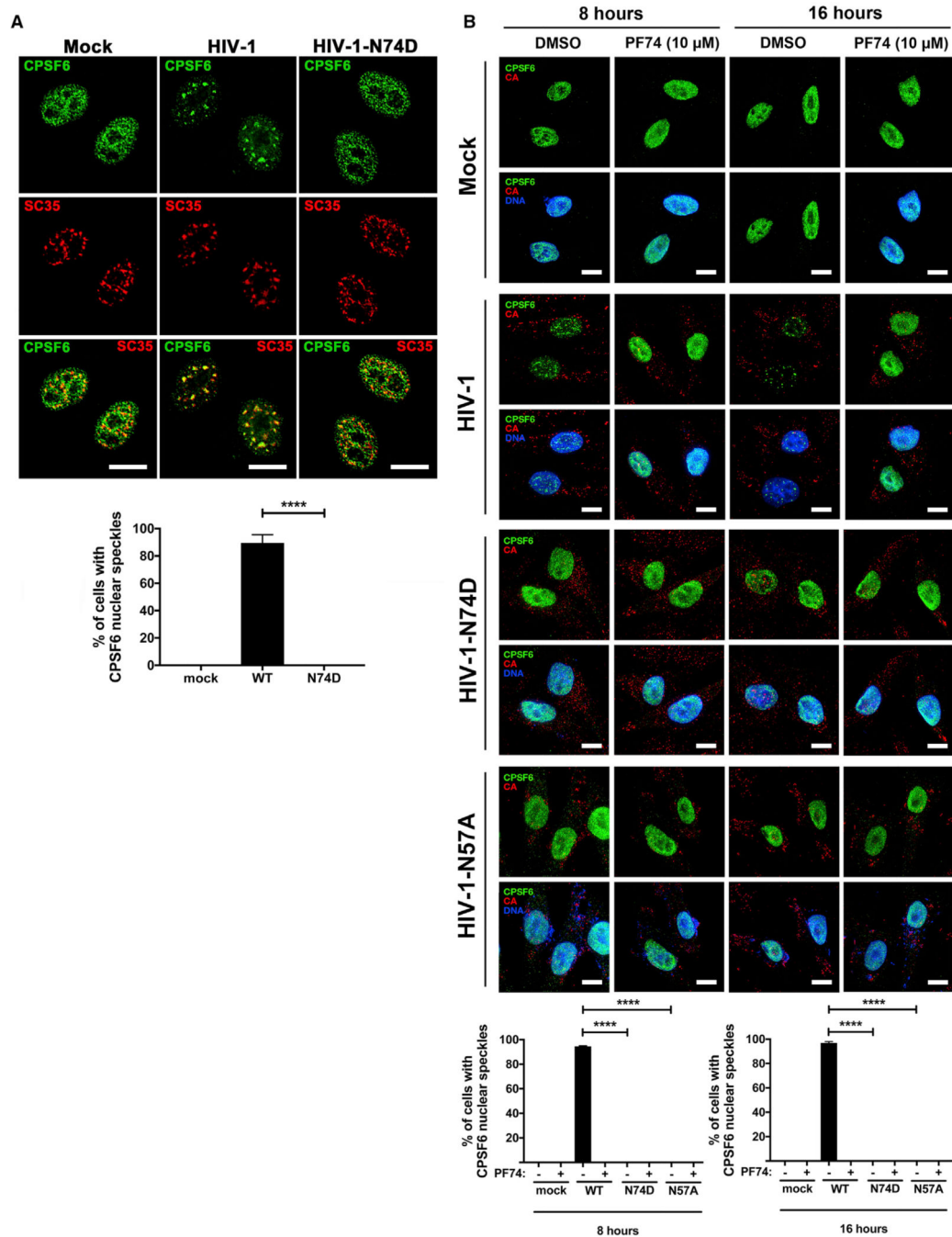
Figure 2. Formation of CPSF6 Speckles in the Nucleus during HIV-1 Infection Requires Interaction with Nuclear Capsid

(A) HeLa cells were infected with wild-type and capsid mutant HIV-1-N74D viruses at an MOI of ~2 for 16 h. Subsequently, fixed and permeabilized samples were immunostained using specific antibodies directed against CPSF6 (green) and SC35 (red). As control, similar immunostaining was performed in mock-infected cells.

(B) HeLa cells were infected with wild-type HIV-1, mutant HIV-1-N74D, mutant HIV-1-N57A viruses at MOI = ~2 in the presence of 10 μM PF74 or DMSO as a vehicle control. 8 or 16 h post-infection, cells were fixed and permeabilized. Samples were immunostained

using specific antibodies directed against CPSF6 and HIV-1 capsid (CA). Cellular nuclei were counterstained with DAPI (DNA). The percentage of cells containing CPSF6 nuclear speckles was determined by visual inspection of 200 cells per sample for three independent experiments.

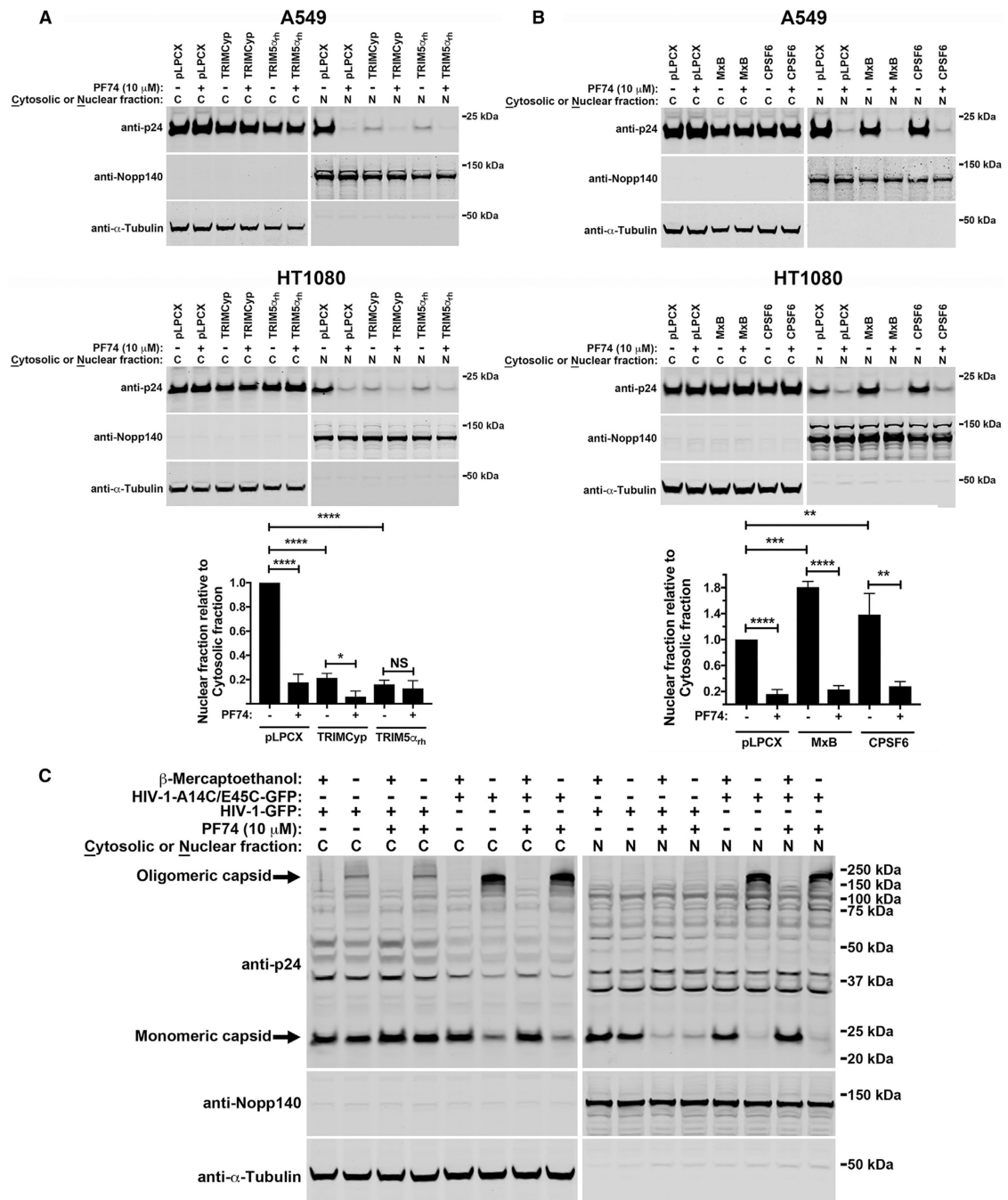****$p < 0.0001$ (as determined by an unpaired t test). Scale bars, 6 μM.

Figure 3. Assembled Capsid Complexes Are Imported into the Nuclear Compartment during HIV-1 Infection

(A and B) A549 or HT1080 cells stably expressing rhesus TRIM5α_{rh} (A), owl monkey TRIMCyp (A), human NES-CPSF6(1–358) (B), human MxB proteins (B), or empty pLPCX vector were infected with wild-type HIV-1-GFP at an MOI of 2 in the presence of 10 μM PF74 for 8 h. Cells were separated into nuclear and cytosolic fractions and analyzed for capsid content by western blotting using anti-p24 antibodies. The ratio of nuclear to cytosolic capsid for three independent experiments with standard deviations is shown. *p <

0.005; **p < 0.001; ***p < 0.0005; ****p < 0.0001; NS, not significant (as determined by the unpaired t test).

(C) Human A549 cells were infected using p24-normalized amounts of wild-type HIV-1-GFP and HIV-1-A14C/E45C-GFP viruses (virus amount corresponded to wild-type MOI = 2) in the presence of 10 μM PF74 for 8 h. Cells were separated into nuclear and cytosolic fractions and analyzed for capsid content by western blotting using anti-p24 antibodies in the presence or absence of the reducing agent β-mercaptoethanol. Experiments were repeated three times (Figure S4), and a representative image is shown.
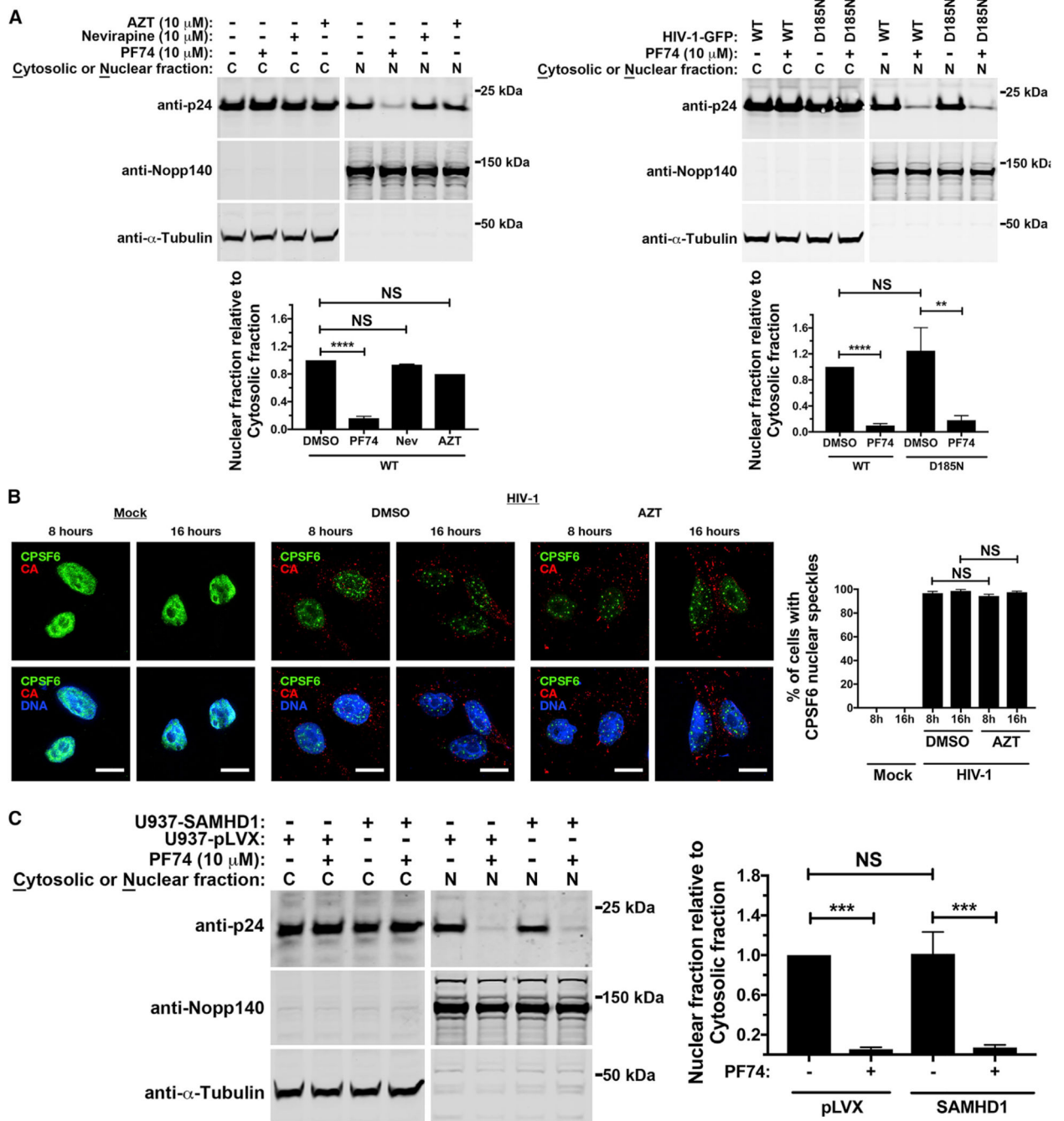
Figure 4. Inhibiting RT Does Not Affect the Levels of Nuclear Capsid during HIV-1 Infection
(A) Human A549 cells were infected with wild-type HIV-1-GFP at an MOI of 2 in the presence of 10 μM PF74, 10 μM AZT, 10 μM nevirapine, or DMSO as a vehicle control for 8 h. Cells were separated into nuclear and cytosolic fractions and analyzed for capsid content by western blotting using anti-p24 antibodies. Similar fractionation experiments were performed in cells infected with p24-normalized HIV-1-GFP and mutant HIV-1-D185N-GFP viruses. The ratio of nuclear to cytosolic capsid for three independent

experiments with standard deviations is shown. **p< 0.001; ****p< 0.0001; NS, not significant (as determined by an unpaired t test).

(B) HeLa cells were infected with wild-type HIV-1 at an MOI of ~2 in the presence of 10 μM AZT. After incubation for 8 or 16 h, cells were fixed, permeabilized, and immunostained for CPSF6 and HIV-1 capsid (CA). Cellular nuclei were counterstained with DAPI. The percentage of cells containing CPSF6 nuclear speckles was determined by visual inspection of 200 cells per sample for three independent experiments. Scale bars, 6 μM.

(C) PMA-treated human U937 Cells stably expressed SAMHD1 or the empty vector pLVX were infected with wild-type HIV-1-GFP at an MOI of 2 in the presence of 10 μM PF74 for 8 h. Cells were separated into nuclear and cytosolic fractions and analyzed for capsid content by western blotting using anti-p24 antibodies. The ratio of nuclear to cytosolic capsid for three independent experiments with standard deviations is shown. ***p < 0.0005; NS, not significant (as determined by an unpaired t test).
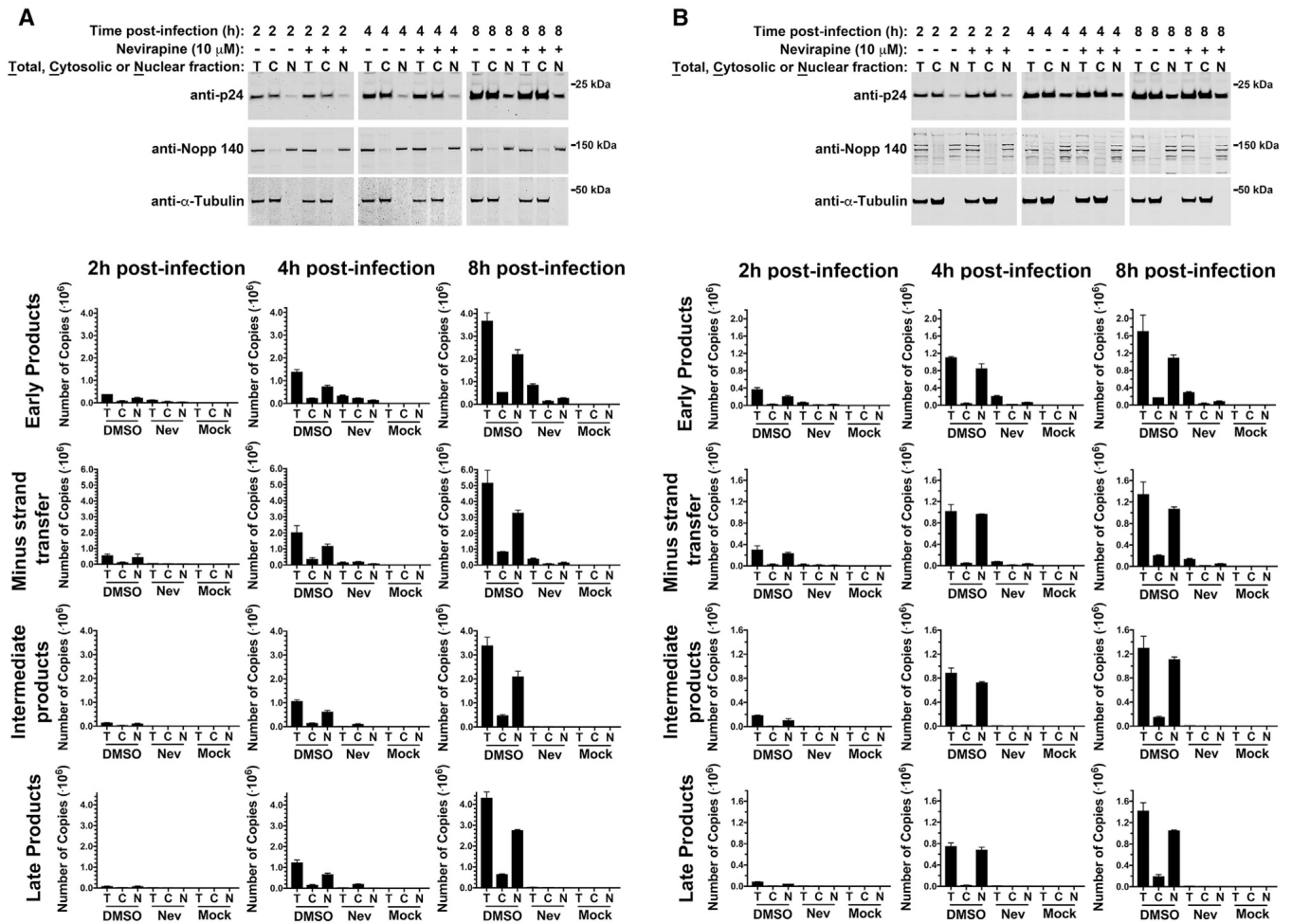
Figure 5. RT Occurs in the Nuclear Compartment

(A and B) A549 (A) and Cf2Th (B) cells were infected with wild-type HIV-1-GFP at an MOI of 2 in the presence of 10 μM nevirapine. After incubation for the indicated times, cells were fractionated, and 10% aliquots of total, cytosolic, and nuclear fractions were analyzed by western blotting using anti-p24, anti-Nopp 140, and anti-α-tubulin antibodies (A and B, upper panels) or used for DNA extraction and analyzed for the presence of HIV-1 RT intermediates (early products, minus-strand transfer, intermediate products, and late products) by quantitative PCR as described in STAR Methods (A and B, lower panels). Experiments were repeated three times (Figures S6 and S7), and representative images with standard deviation are shown.

KEY RESOURCES TABLE

REAGENT or RESOURCE	SOURCE	IDENTIFIER
Antibodies		
Human monoclonal anti-HIV-1 p24 (71-31)	NIH AIDS Reagent Program	Cat# 530; RRID:AB_1840889
Mouse monoclonal anti-HIV-1 p24 (183-H12-5C)	NIH AIDS Reagent Program	Cat 3537; RRID:AB_2832923
Rabbit monoclonal anti-hemagglutinin (HA) (RM305)	Novus	Cat# NBP2-61477; RRID:AB_2744968
Mouse monoclonal anti-CPSF6 (human) (3F11)	Novus	Cat# H00011052-M10; RRID:AB_606091
Mouse monoclonal anti-SC-35 (1SC-4F11)	Sigma-Aldrich	Cat# 04-1550; RRID:AB_11212756
Mouse monoclonal anti-glyceraldehyde-3-phosphate dehydrogenase (GAPDH)	Invitrogen (Thermo Fisher Scientific)	Cat# AM4300; RRID:AB_2536381
Rabbit polyclonal anti-alpha Tubulin	Invitrogen	Cat# PA5-29444; RRID:AB_2546920
Mouse monoclonal anti-FLAG M2	Sigma-Aldrich	Cat# F1804; RRID:AB_262044
Mouse monoclonal anti-hemagglutinin (HA)	Sigma-Aldrich	Cat# H3663; RRID:AB_262051
Rabbit polyclonal anti-Nopp140 (human) (RS8 serum)	Kittur et al., 2007 College of Medicine	Gift of U. Thomas Meier, Albert Einstein
Goat anti-Mouse IRDye 680LT	LI-COR	Cat# 925-68020; RRID:AB_10706161
Goat anti-Rabbit IRDye 680LT	LI-COR	Cat# 926-68021; RRID:AB_2713919
Goat anti-Mouse IRDye 800CW	LI-COR	Cat# 926-32210; RRID:AB_2687825
Goat anti-Rabbit IRDye 800CW	LI-COR	Cat# 925-32211; RRID:AB_621843
Bacterial and Virus Strains		
E. Coli DH5α competent cells	Zymo Research	Cat# T3007
HIV-1 $_{NL4-3}$	Selyutina et al., 2020	N/A
HIV-1-N57S	This paper	N/A
HIV-1-N74D	This paper	N/A
HIV-1-A14C/E45C	This paper	N/A
HIV-1-D185N	This paper	N/A
Chemicals, Peptides, and Recombinant Proteins		
Dimethyl sulfoxide (DMSO)	Sigma-Aldrich	Cat#: D2438; CAS: 67-68-5
Difco LB Broth, Miller (Luria-Bertani)	Fisher Scientific	Cat#: BD244610
Tris (TRIS(HYDROXYMETHYL) AMINOMETHANE)	Crystalgen	Cat#: 300-844-5000; CAS: 77-86-1
cOmplete EDTA-free protease inhibitor cocktail	Millipore Sigma	Cat#: 11873580001
Sodium Chloride (NaCl)	Crystalgen	Cat# 300-747-5000; CAS: 767-14-5
β-Mercaptoethanol (BME)	Acros organics	Cat# 125470010; CAS: 60-24-2

REAGENT or RESOURCE	SOURCE	IDENTIFIER
2-(N-morpholino) ethanesulfonic acid (MES)	Calbiochem	Cat# 475893; CAS: 4432-31-9
Magnesium Chloride (MgCl$_2$)	Sigma-Aldrich	Cat# M2670; CAS: 7791-18-6
Potassium Chloride (KCl)	Fisher Scientific	Cat# BP366-1; CAS: 7447-40-7
Dithiothreitol (DTT)	VWR	Cat# 97061-340; CAS: 3483-12-3
D-(+)-Sucrose	VWR	Cat# 97061-432; CAS: 57-50-1
Dulbecco's Phosphate-Buffered Salt (PBS) Solution 1X	Corning	21031CV
EDTA, pH 8.0, 0.5M	Corning	46034CI
Paraformaldehyde (4% in PBS)	Boston BioProducts	Cat# BM-155
PF74	Sigma Aldrich	Cat# SML0835
Nevirapine	NIH AIDS Reagent Program	Cat# 4666
Zidovudine (AZT)	NIH AIDS Reagent Program	Cat# 3485
Poly-L-Lysine (0.01% solution)	Sigma	Cat# P4707
Critical Commercial Assays		
QuikChange II site-directed mutagenesis kit	Agilent	Cat#: 200523
QIAamp DNA Micro Kit	QIAGEN	Cat# 56304
Experimental Models: Cell Lines		
Human: MOLT-3	ATCC	CRL-1552
Human: 293T/17	ATCC	CRL-11268
Human: A549	ATCC	CCL-185
Human: HeLa	ATCC	CCL-2
Human: HT1080	ATCC	CCL-121
Canine: Cf2Th	ATCC	CRL-1430
Oligonucleotides		
All standard cloning primers for site-directed mutagenesis	Integrated DNA Technologies	N/A
Early reverse transcripts (ERT) hRU5-F2 5′-GCCTCAATAAAGCTTGCCTTGA-3′	Mbisa et al., 2009	
Early reverse transcripts (ERT) hRU5-R 5′-TGACTAAAAGGGTCTGAGGGATCT-3′	Mbisa et al., 2009	N/A
ERT probe hRU5-P: 5′-(FAM)-AGAGTCACACAACAGACGGGCACACACTA-(TAMRA)-3′	Mbisa et al., 2009	N/A
Minus strand transfer FST-F1: 5′-GAGCCCTCAGATGCTGCATAT-3′	Mbisa et al., 2009	N/A
Minus strand transfer SS-R4: 5′-CCACACTGACTAAAAGGGTCTGAG-3′	Mbisa et al., 2009	N/A
Minus strand transfer probe P-HUS-SS1: 5′-(FAM)-TAGTGTGTGCCCGTCTGTTGTGTGAC-(TAMRA)-3′	Mbisa et al., 2009	N/A
Intermediate products GagF1: 5′-CTAGAACGATTCGCAGTTAATCCT-3′	Mbisa et al., 2009	N/A
Intermediate products GagR1: 5′-CTATCCTTTGATGCACACAATAGAG-3′	Mbisa et al., 2009	N/A

REAGENT or RESOURCE	SOURCE	IDENTIFIER
Intermediate products probe P-HUS-103: 5′-(FAM)-CATCAGAAGGCTGTAGACAAATACTGGGA-(TAMRA)-3′	Mbisa et al., 2009	N/A
Table S1 Primers	N/A	N/A
Recombinant DNA		
pLPCX	Clontech	Cat# 631511
pLPCX-TRIMCyp-HA	Stremlau et al., 2006	N/A
pLPCX-CPSF6(1-358)-FLAG	Fricke et al., 2013	N/A
pLPCX-MxB-FLAG	Fricke et al., 2014a	N/A
pLPCX-TRIM5α_{rh}-HA	Stremlau et al., 2006	N/A
Plasmid: Tat	Stremlau et al., 2006	N/A
Plasmid: Rev	Stremlau et al., 2006	N/A
Plasmid: VSVg	Stremlau et al., 2006	N/A
pVPack-GP	Agilent	Cat #: 217566
pVPack-VSV-G	Agilent	Cat #: 217567
Other		
TURBO DNase (2 U/µL)	Invitrogen	Cat#AM2238
Fetal Bovine Serum (FBS, heat-inactivated)	GIBCO	16140-071
RPMI-1640 (high glucose)	Corning	MT10-017-CV
Penicillin-streptomycin (5 mg/mL)	Corning	MT10-040-CV
Sodium pyruvate (100x)	Corning	MT25-000-CI
HEPES (100x)	Fisher / HyClone	SH3023701
DMEM (high glucose)	Corning	MT10-017-CV